



# 1 Evaluating Trends and Seasonality in Modeled PM<sub>2.5</sub> 2 Concentrations Using Empirical Mode Decomposition

3 Huiying Luo<sup>1</sup>, Marina Astitha<sup>1\*</sup>, Christian Hogrefe<sup>2</sup>, Rohit Mathur<sup>2</sup>, S. Trivikrama Rao<sup>1,3</sup>

4 <sup>1</sup>University of Connecticut, Department of Civil and Environmental Engineering, Storrs-Mansfield, CT, USA

5 <sup>2</sup>U.S. Environmental Protection Agency, Research Triangle Park, NC, USA

6 <sup>3</sup>North Carolina State University, Raleigh, NC, USA

7 \*Corresponding author: Marina Astitha, Civil and Environmental Engineering, University of Connecticut, 261

8 Glenbrook Road, Storrs, CT, 06269-3037, Phone: 860-486-3941, Fax: 860-486-2298, Email:

9 [marina.astitha@uconn.edu](mailto:marina.astitha@uconn.edu).

10 **Abstract.** Regional-scale air quality models are being used for studying the sources, composition, transport,  
11 transformation, and deposition of fine particulate matter (PM<sub>2.5</sub>). The availability of decadal air quality simulations  
12 provides a unique opportunity to explore sophisticated model evaluation techniques rather than relying solely on  
13 traditional operational evaluations. In this study, we propose a new approach for process-based model evaluation of  
14 speciated PM<sub>2.5</sub> using improved Complete Ensemble Empirical Mode Decomposition with Adaptive Noise (improved  
15 CEEMDAN) to assess how well version 5.0.2 of the coupled Weather Research and Forecasting model - Community  
16 Multiscale Air Quality model (WRF-CMAQ) simulates the time-dependent long-term trend and cyclical variations in  
17 the daily average PM<sub>2.5</sub> and its species, including sulfate (SO<sub>4</sub>), nitrate (NO<sub>3</sub>), ammonium (NH<sub>4</sub>), chloride (Cl) organic  
18 carbon (OC) and elemental carbon (EC). The utility of the proposed approach for model evaluation is demonstrated  
19 using PM<sub>2.5</sub> data at three monitoring locations. At these locations, the model is generally more capable of simulating  
20 the rate of change in the long-term trend component than its absolute magnitude. Amplitudes of the sub-seasonal and  
21 annual cycles of total PM<sub>2.5</sub>, SO<sub>4</sub> and OC are well reproduced. However, the time-dependent phase difference in the  
22 annual cycles for total PM<sub>2.5</sub>, OC and EC reveal a phase shift of up to half year, indicating the need for proper temporal  
23 allocation of emissions and for updating the treatment of organic aerosols compared to the model version used for this  
24 set of simulations. Evaluation of sub-seasonal and inter-annual variations indicates that CMAQ is more capable of  
25 replicating the sub-seasonal cycles than inter-annual variations in magnitude and phase.

## 26 **Keywords**

27 Model evaluation, coupled WRF-CMAQ, improved Complete Ensemble Empirical Mode Decomposition (EMD)  
28 with Adaptive Noise, Speciated PM<sub>2.5</sub>, Scale Separation, Seasonality, Trend

29



## 30 **1 Introduction**

31 It is well recognized that inhalable fine particulate matter ( $PM_{2.5}$ ) adversely impacts human health and the  
32 environment. Regional-scale air quality models are being used in health impact studies and decision-making related  
33 to  $PM_{2.5}$ . Long-term model simulations of  $PM_{2.5}$  concentrations using regional air quality models are essential to  
34 identify long-term trends and cyclical variations such as annual cycles in areas larger than what is covered by in-situ  
35 measurements. However, total  $PM_{2.5}$  concentrations are challenging to predict because of the dependence on the  
36 contributions from individual  $PM_{2.5}$  components, such as sulfates, nitrates, carbonaceous species, and other natural  
37 species. In this context, a detailed process-based evaluation of the simulated speciated  $PM_{2.5}$  must be carried out to  
38 ensure acceptable replication of observations so model users can have confidence in using regional air quality models  
39 for policy-making. Furthermore, process based information can be useful for making improvements to the model.

40 Some of the trend or step change evaluations of regional air quality models in the past have focused on specific pairs  
41 of years (Kang et al., 2013; Zhou et al., 2013; Foley et al., 2015). These studies do not properly account for the sub-  
42 seasonal and inter-annual variations between those specific periods. Trend evaluation is commonly done by linear  
43 regression of indexes such as the annual mean or specific percentiles, assuming linearity and stationarity of time series  
44 (Civerolo et al., 2010; Hogrefe et al., 2011; Banzhaf et al., 2015; Astitha et al., 2017). The problem with the linear  
45 trend evaluation is that there is no guarantee the trend is actually linear during the period of the study because the  
46 underlying processes are in fact nonlinear and nonstationary (Wu et al., 2007).

47 Seasonal variations are usually studied and evaluated by investigating the monthly or seasonal means (Civerolo et al.,  
48 2010; Banzhaf et al., 2015; Yahya et al., 2016; Henneman et al., 2017). Evaluation of ten-year averaged monthly mean  
49 of  $PM_{2.5}$  simulated with WRF/Chem against the Interagency Monitoring of Protected Visual Environments  
50 (IMPROVE) by Yahya et al. (2016) shows that the model captures the observed features of summer peaks in  $PM_{2.5}$   
51 with a phase shift of few months. However, according to the analysis (Fig. 10) in Henneman et al. (2017), the  
52 seasonality shown in monthly-averaged  $PM_{2.5}$  time series is much less distinguishable compared with that of ozone  
53 and CMAQ (version 5.0.2) does not replicate the monthly  $PM_{2.5}$  quite well with large underestimation in the summer  
54 months. In these studies, the seasonality might not be well represented by the preselected averaging window size of  
55 one or three months. In addition, averaging of those monthly or seasonal means across multiple years may conceal the  
56 long-term trends or interannual variations driven by climate change, emission control policies or other slow varying  
57 processes.

58 To address the above-mentioned problems, we propose a new method for conducting air quality model evaluation for  
59  $PM_{2.5}$  using improved CEEMDAN. Improved CEEMDAN is an Empirical Mode Decomposition (EMD)-based, data-  
60 driven intrinsic mode decomposition technique that can adaptively and recursively decompose a nonlinear and  
61 nonstationary signal into multiple modes called intrinsic mode functions (IMFs) and a residual (trend component)  
62 (Huang et al., 1998; Wu and Huang, 2009; Yeh et al., 2010; Torres et al., 2011; Colominas et al., 2014). It does not  
63 require any preselection of the temporal scales or assumptions of linearity and stationarity for the data, thereby  
64 providing some insights into time series of  $PM_{2.5}$  concentrations and its components. Decomposed  $PM_{2.5}$  long-term  
65 trend components and annual cycles from observed and simulated  $PM_{2.5}$  serve as the intuitive carrier of the trend and



66 seasonality evaluation. In the meantime, several other IMFs with characteristic time scales ranging from multiple days  
67 to years are also decomposed, enabling model evaluation of the less studied sub-seasonal and inter-annual variations.

68 Section 2 describes the coupled WRF-CMAQ model simulations and corresponding observations from multiple  
69 speciated  $PM_{2.5}$  networks. Section 3 presents an overview of the EMD and improved CEEMDAN technique and the  
70 statistical metrics accompanying model evaluation, including the time-dependent intrinsic correlation (TDIC) on the  
71 decomposed IMFs (Chen et al., 2010; Huang and Schmitt, 2014; Derot et al., 2016). Section 4 describes the findings  
72 on the long-term trend and seasonality in total  $PM_{2.5}$  and its components, as resolved by the improved CEEMDAN  
73 technique and includes a discussion on the sub-seasonal, seasonal, and inter-annual variability. The conclusions from  
74 this work are presented in section 5.

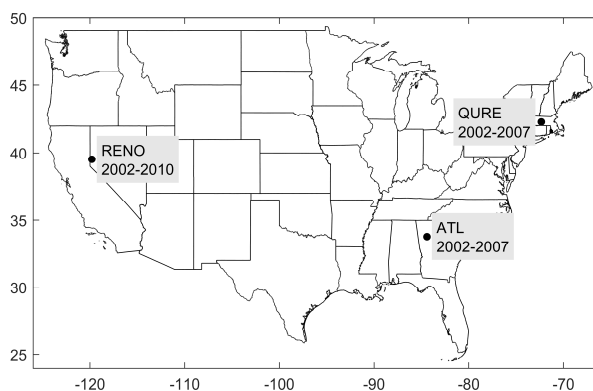
## 75 **2 Coupled WRF-CMAQ $PM_{2.5}$ Simulations and Observations**

76 The two-way coupled WRF-CMAQ (version 5.0.2) is configured with a 36 km horizontal grid spacing over the  
77 contiguous United States (CONUS) with 35 vertical layers of varying thickness extending from the surface to 50 mb  
78 (Wong et al., 2012; Gan et al., 2015). Time-varying chemical lateral boundary conditions were derived from the 108  
79 km resolution hemispheric WRF-CMAQ (Mathur et al., 2017) simulation for the 1990-2010 period (Xing et al., 2015).  
80 The simulations are driven by a comprehensive emission dataset which includes the aerosol precursors and primary  
81 particulate matter (Xing et al., 2013, 2015). The readers can refer to Gan et al. (2015) for additional model information  
82 and the trend evaluation against seven pairs of sites from the CASTNET (Clean Air Status and Trend Network) and  
83 IMPROVE networks for 1995-2010. We obtained the 2002-2010 daily average  $PM_{2.5}$  and its speciated time series  
84 from the set of simulations with direct aerosol feedback. The earlier years of 1990-2001 are not included in this  
85 evaluation because of the limited availability of speciated  $PM_{2.5}$  observations.

86 To avoid misinterpretation of data due to the presence of missing values, only sites with continuous complete long-  
87 term record for total  $PM_{2.5}$  and its speciation including  $SO_4$ ,  $NO_3$ ,  $NH_4$ , OC, EC, and Cl are studied (Fig. 1). All of the  
88 selected sites have data coverage above 90% each year for at least six consecutive years between 2002 and 2010  
89 (equivalent to 30% for 1-in-3 days sampling sites). This strict data selection led to the sparsity of this type of  
90 observations for the study period. QURE, a rural site carrying out 1-in-3 days sampling of total and speciated  $PM_{2.5}$   
91 of  $SO_4$ ,  $NO_3$ , OC, EC, and Cl, is located in Quabbin Summit, MA. It is one of the three sites from the IMPROVE  
92 network that has at least six continuous years of speciated observations and was selected here to demonstrate the  
93 application of the proposed method in rural areas. It should be noted that the majority of the observed Cl in 2002 and  
94 2003 is negative due to a filter issue problem which was not addressed until 2004 (White, 2008). Thus, simulations of  
95 Cl are only evaluated during 2004-2007 at this site. Station RENO, located in urban Reno, NV, is also a 1-in-3 days  
96 sampling site of total and speciated  $PM_{2.5}$  of  $SO_4$ ,  $NO_3$ ,  $NH_4$ , OC, and EC, and it is the only Chemical Speciation  
97 Network (CSN) site that fulfills this data coverage requirement. The third site ATL in the Southeastern Aerosol  
98 Research and Characterization Study (SEARCH) network is located 4.2 km northwest of downtown Atlanta, GA. It  
99 is the only long-term site available with daily sampling rate (Hansen et al., 2003; Edgerton et al., 2005) that meets the  
100 data coverage requirement. The best-estimate (BE), a calculated concentration intended to represent what is actually



101 in the atmosphere (Edgerton et al., 2005), of the total PM<sub>2.5</sub> and SO<sub>4</sub>, NO<sub>3</sub>, NH<sub>4</sub>, and EC components are retrieved for  
102 the evaluation. OC component is a direct measurement. These three sites have a continuous record covering at least 6  
103 years (2002 – 2007 for QURE and ATL and 2002 – 2010 for RENO) that allows an evaluation of long-term trends.



104

105 **Fig. 1. Location and data coverage of the PM<sub>2.5</sub> monitoring sites QURE, RENO and ATL.**

### 106 **3 Methodology**

#### 107 **3.1 Empirical Mode Decomposition**

108 The Empirical Mode Decomposition (EMD) technique, proposed in the late 1990s, is capable of adaptively and  
109 recursively decomposing a signal into multiple modes called intrinsic mode functions (IMFs), where each mode has  
110 a characteristic frequency, and a residual with at most one extremum (Huang et al., 1998). The decomposed signal  
111 then is expressed as the summation of all IMFs and the residual:

$$112 \quad x = \sum_{i=1}^k d_i + r \quad (1)$$

113 where  $x$  is the original signal,  $d_i$  is the  $i^{\text{th}}$  IMF,  $k$  is the number of the IMFs and  $r$  is the final residual. Each IMF has  
114 the following properties (Huang et al., 1998):

115 1) The number of extrema (maxima and minima) and the number of zero-crossings must be equal or differ at most by  
116 one;

117 2) The local mean at any point, the mean of the envelope defined by local maxima and the envelope defined by local  
118 minima, must be zero.

119 Nevertheless, “mode mixing” where oscillations with very disparate scales can be present in one mode or vice versa  
120 is commonly reported. To cope with this issue, multiple noise assisted EMD have been developed successively (Wu  
121 and Huang, 2009; Yeh et al., 2010; Torres et al., 2011; Colominas et al., 2014). It is evident that the latest improved  
122 Complete Ensemble EMD with Adaptive Noise (improved CEEMDAN) manages to alleviate the problem of mode  
123 mixing with the benefit of reducing the amount of noise presented and avoiding spurious modes (Colominas et al.,



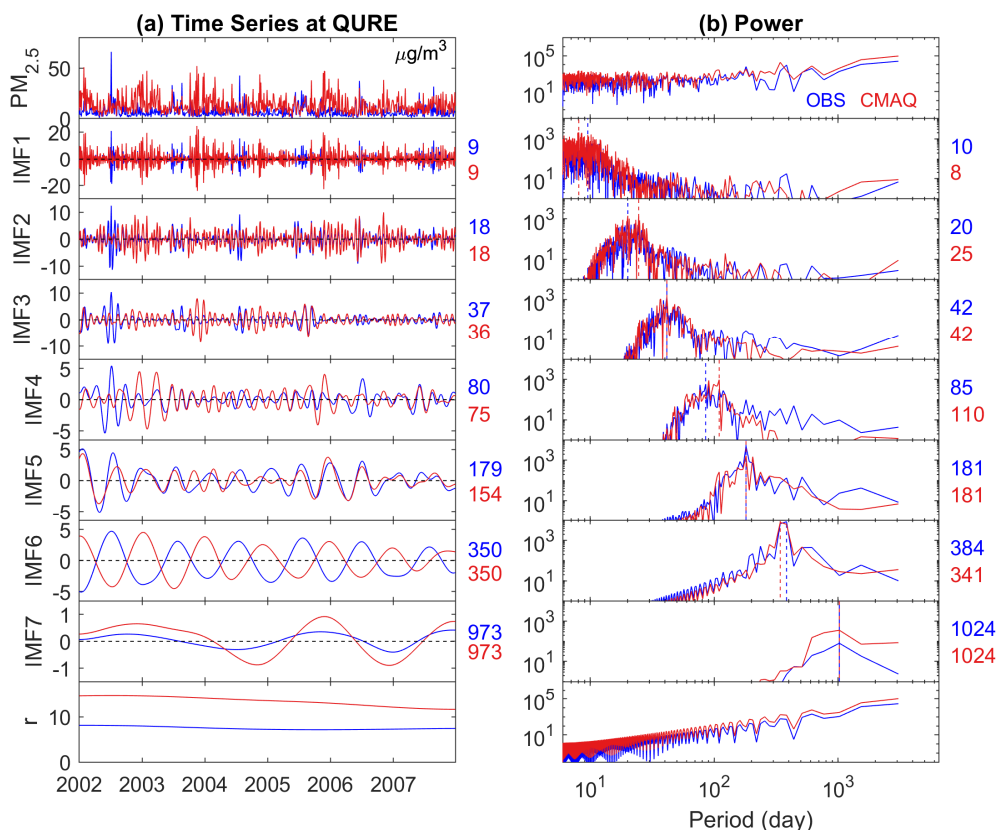
124 2014). Moreover, the end effects or boundary effects have been addressed by its predecessor EEMD (Ensemble  
125 Empirical Mode Decomposition) by extrapolating the maxima and minima, and behaved well in numerous time series  
126 with dramatically variant characteristics (Wu and Huang, 2009). The extrapolation of maxima and minima is proven  
127 to be more effective compared with the extrapolation of the signal itself such as repetition or reflection (Rato et al.,  
128 2008).

129 Given the EMD's ability to deal with real-world nonstationary and nonlinear time series data, it is widely used in  
130 engineering, economics, earth and environmental sciences (e.g., Huang et al., 1998; Chang et al., 2003; Yu et al., 2008;  
131 Colominas et al., 2014; Derot et al., 2016). We use the most up-to-date noise-assisted improved CEEMDAN technique  
132 with at least hundreds of noise realizations to decompose observed and simulated PM<sub>2.5</sub> time series. Readers can refer  
133 to Colominas et al. (2014) for detailed description of the technique and access to the corresponding MATLAB code.  
134 Trial and error attempts are made in setting the input of the improved CEEMDAN function to achieve best mode  
135 separation.

136 The impact of boundaries on the decomposed annual cycles and the residual is assessed by the variations (standard  
137 deviation) of hypothetical decomposed boundaries by cutting a continuous eighteen-year total PM<sub>2.5</sub> observation  
138 (North Little Rock, AR) 48 times at different years and times of the year (Fig. S1). The standard deviation is found to  
139 largely diminish within half the annual cycles and could be negligible within one year for the annual cycle. This could  
140 very possibly expand to IMFs with other characteristic scales. Yet, trend components (residuals) show variability  
141 depending on the available time period after cutting. Most of the time, they follow the reference long-term trend  
142 reflected either by the residual or the summation of the residual and the IMF with longest temporal scale decomposed  
143 from the eighteen-year PM<sub>2.5</sub> (Fig. S1c). This is in line with our expectations as a trend should exist within a given  
144 time span, following the definition in Wu et al. (2007): "The trend is an intrinsically fitted monotonic function or a  
145 function in which there can be at most one extremum within a given data span". Although very strict data completeness  
146 requirement is employed for this study, it should not be conceived as a limitation of the method itself. A sensitivity  
147 test based on a period of nine years of total PM<sub>2.5</sub> observation at the same site with 99% data coverage shows that even  
148 though variability of annual cycles and long-term trends increases with decreased data availability (100%, 90%, ...,  
149 10%), the structure of those components is consistent. The average of 40 realizations of annual cycles and long-term  
150 trend components in each data-completeness scenario is in perfect alignment with that of 100% data completeness  
151 (Fig. S2 and S3). Given the fact that those 40 realizations in each scenario are based on independent random samplings  
152 of the original observations, the increased variability could very possibly result from the difference in the sampled  
153 data itself rather than the method. Thus, the robustness of improved CEEMDAN decomposed annual cycles and long-  
154 term trend is justified. In fact, EMD has been proven to be an effective tool for data gap-filling (Moghtaderi et al.,  
155 2012).

156

157



158

159 **Fig. 2.** Decomposition of observed (blue) and simulated (red) 24-hour average total PM<sub>2.5</sub> into 7 IMFs and a  
 160 residual component (trend) at Quabbin Summit, MA using the improved CEEMDAN: (a) Time series of total  
 161 PM<sub>2.5</sub>, IMFs and the residual component (all with unit of µg/m<sup>3</sup>); (b) Power spectrum of the corresponding  
 162 time series. The colored numbers on the right side of time series are the mean period  $t_m$  in days, while the ones  
 163 on the right side of the power spectrum are the peak period  $t_p$  in days, which are also indicated by the dashed  
 164 vertical lines on the power spectrum. Note that the scales for the time series are not all the same. Also, all power  
 165 spectra are in the log scale and those of the IMFs are zoomed in with a range of 10<sup>0</sup> to 10<sup>4</sup> on the y-scale for  
 166 better visual clarity (compared with 10<sup>-2</sup> to 10<sup>7</sup> for total PM<sub>2.5</sub> and the residual component).

167

168 The characteristic period of each IMF can be estimated by the peak period  $t_p$  (days) where the power spectrum  
 169 of the IMF peaks:

170 
$$t_p = \frac{1}{f_p} \quad (2)$$

171 in which  $f_p$  is the frequency that the power spectrum peaks in the unit of number of cycles per day. The peak estimates  
 172 can be biased if more than one high-power frequency is located close to each other in one IMF. Thus, power spectrum



173 is only used as a fast screening tool to determine if a desired decomposition is accomplished. As an alternative  
174 approach, the mean period  $t_m$  can be estimated by:

$$175 \quad t_m = \frac{\text{Time span}}{(n_{max} + n_{min} + n_{zero})/4} \quad (3)$$

176 where  $n_{max}$ ,  $n_{min}$  and  $n_{zero}$  are the number of maxima, minima and zero-crossings, respectively, during the  
177 *Time span* (days). As the frequency decreases, the mean period estimates become less accurate because of the limited  
178 time span compared with the length of the cycle and should be carefully interpreted.

179 An example of the total  $PM_{2.5}$  decomposition with improved CEEMDAN at the QURE site shows modes ranging from  
180 very high frequency to very low frequency (IMF1 to IMF7) and a residual (Fig. 2). Mean ( $t_m$ ) and peak ( $t_p$ )  
181 estimations of the characteristic periods of each IMF are presented on the right side of each mode. Annual cycles and  
182 long-term trend components are well represented by IMF6 and the residual, with the remaining IMFs carrying weekly,  
183 sub-seasonal, seasonal, and inter-annual variations, respectively, for both observed and simulated  $PM_{2.5}$  (Fig. 2). We  
184 have noticed that in some rare cases, a spurious mode in the last IMF with synchronous signal and very close scales  
185 to its previous IMF exists. This is possibly due to the fact that the characteristic periods of those IMFs are in proximity  
186 to the span of the studied time span. In these cases, the last two modes are merged by adding those two modes together  
187 to conduct a detailed evaluation as discussed in Section 4.

### 188 3.2 Statistical metrics

189 EMD-decomposed IMFs and trend components allow for a detailed time-dependent evaluation of  $PM_{2.5}$  and provide  
190 a novel opportunity to trace the performances of specific scales back to the corresponding speciated components. Note  
191 that the trend component is the decomposed residual component from the  $PM_{2.5}$  in the unit of  $\mu\text{g}/\text{m}^3$  and it is not the  
192 traditional concept of trend in concentration per time. In addition to a direct evaluation of its magnitude, we also  
193 calculated its derivative to identify the periods with higher or lower rate of change (concentration per time). Time-  
194 dependent intrinsic correlation (TDIC) is utilized to study the evolvement of the model performance for cyclic  
195 variations throughout time (Chen et al., 2010; Huang and Schmitt, 2014; Derot et al., 2016). It is a set of correlations  
196 calculated for IMFs over a local period of time  $I$  centered around time  $t$ :

$$197 \quad I(t) = [t - \frac{t_w}{2}, t + \frac{t_w}{2}] \quad (4)$$

198 in which  $t$  is the center time for the calculation of the correlation and  $t_w$  is the moving window length. The minimum  
199 of  $t_w$  is set to be the local instantaneous period of the IMF (larger of that in observation or simulation) using the  
200 general zero crossing method to ensure that at least one instantaneous period is included in calculating the local  
201 correlation coefficient (Chen et al., 2010). The maximum of  $t_w$  is the entire data period with a traditional overall  
202 correlation being calculated. The empty spaces in the pyramids used to depict the TDIC are an indication that the  
203 correlation is not statistically significantly different from zero. With both decomposed observed and modeled  
204 concentrations in a narrow scale range, the correlation would no longer be contaminated by coexisting signals of  
205 different scales (Chen et al., 2010).





206 In order to summarize the performance of the decomposed trend component and IMFs, the ratio of the mean  
207 magnitudes of the trend components is defined as:

$$208 \quad r_{trend} = \frac{Mean_{CMAQ}}{Mean_{observation}} \quad (5)$$

209 where  $Mean_{CMAQ}$  and  $Mean_{observation}$  represent the mean of simulated and observed residual components  
210 respectively. The ratio of the mean amplitude of each IMF is defined by Equation 6, where an example for the annual  
211 cycles is provided:

$$212 \quad r_{annual} = \frac{RMS_{CMAQ,annual}}{RMS_{observation,annual}} \quad (6)$$

213 where  $RMS_{observation,annual}$  and  $RMS_{CMAQ,annual}$  represent the root mean square of observed and simulated annual  
214 cycles respectively. Finally, the phase shift of an IMF  $n$  is defined to be days an IMF decomposed from modeled time  
215 series has to shift in order to achieve the highest correlation ( $R_{max}$ ) with the corresponding IMF with similar scale  
216 from observed  $PM_{2.5}$  time series. In practice,  $n$  could be as much as a few cycles of the mean period,  $t_m$ . Here, we  
217 limit the absolute number of shift days to not exceed a half cycle as a reference for the phase shift of an IMF. Thus,  $n$   
218 satisfies  $-(t_m/2) \leq n \leq (t_m/2)$  with  $t_m$  being the larger mean period in observation or simulation. It becomes  
219  $-0.5 \leq n/t_m \leq 0.5$  in terms of number of cycles.

## 220 **4 Results and Discussion**

### 221 **4.1 Temporal scales**

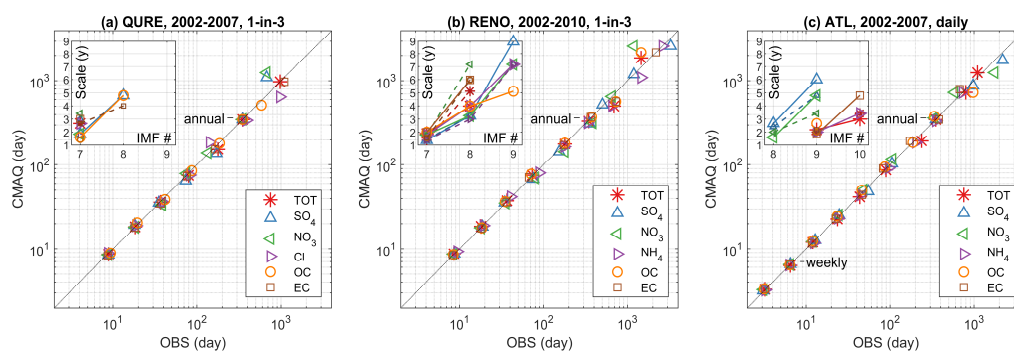
222 Temporal scales in  $PM_{2.5}$  resolved by EMD depend solely on the intrinsic properties of the data itself. These properties  
223 include underlying characteristics of specific  $PM_{2.5}$  concentrations, the data sampling frequency, which determines the  
224 scales that can be resolved in the high frequency IMFs, and the time span for the data coverage, which could possibly  
225 play an important role in differentiating the low frequency IMFs from the trend component. Here, we first evaluate  
226 the scales represented by the mean period in the speciated  $PM_{2.5}$  time series. Note that the mean period is only one  
227 indication of the model evaluation against observations, and it does not indicate any information on the magnitude or  
228 the phase of the time series, which will be further discussed in Sections 4.3 to 4.4.

229 Fig. 3a presents the characteristic scales of IMFs in observed and simulated total and speciated  $PM_{2.5}$  of QURE. The  
230 CMAQ model compares well with the observations for IMFs 1 through 6 with cycles of 9, 19, 37, 78, 158 and 347  
231 days (average of all observed and simulated total and speciated  $PM_{2.5}$ ). Among all these IMFs, IMF6, which represents  
232 the annual cycles, shows the least variations in the characteristic scale (Fig. 3a) and highest peak energy from the  
233 power spectrum such as Fig. 2b for total  $PM_{2.5}$ , except for observed EC and OC where the power of half-year cycles  
234 is more dominant (Fig. S4). These two features demonstrate a clear seasonality in both observed and simulated total  
235 and speciated  $PM_{2.5}$ , which would otherwise be concealed by practices such as monthly averaging. This can be further  
236 confirmed by the statistically significant annual cycles (except for observed EC and OC) (Fig. S5) based on a Monte  
237 Carlo verified relationship between the energy density and mean period of IMFs (Wu and Huang, 2004; Wu et al.,





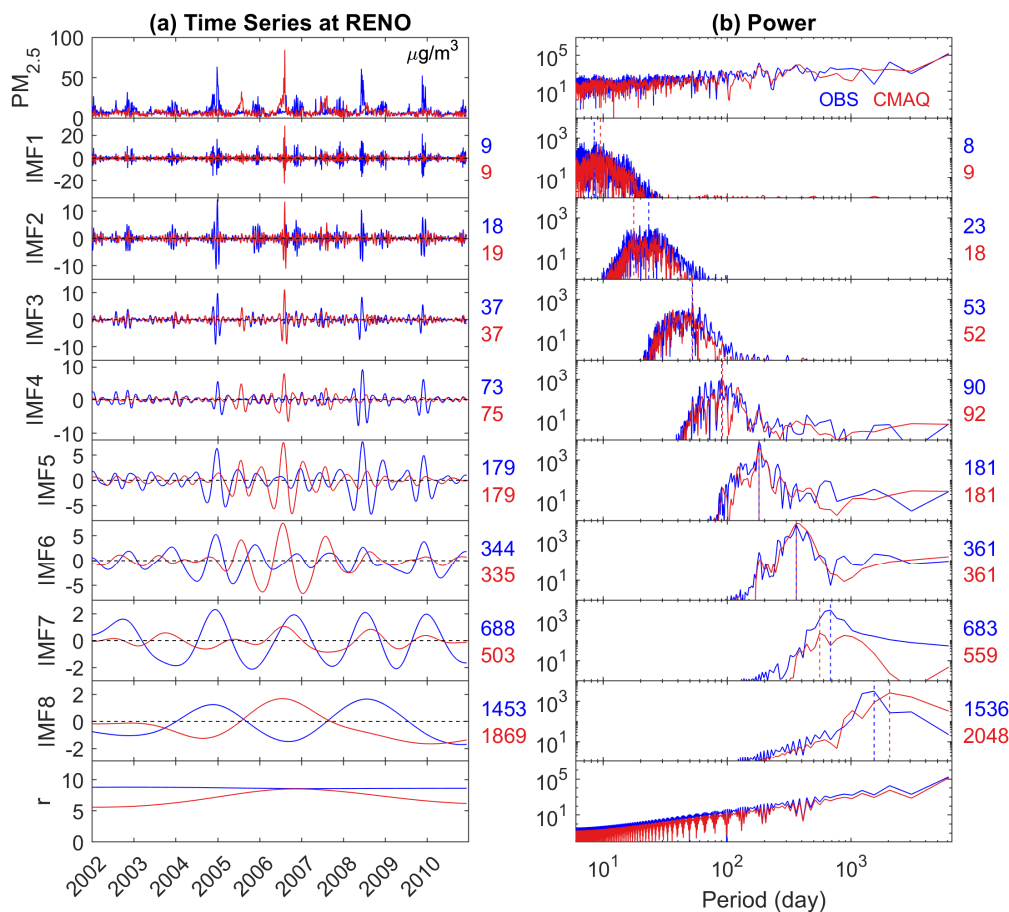
238 2007). To explore the inter-annual cycles in more detail, mean periods of IMFs with scales longer than a year are  
239 being displayed in the top left panel of Fig. 3a. Some variability exists between the observation and model simulation  
240 to the extent that not all IMFs from observation are being simulated and vice versa. The estimated mean periods of  
241 the inter-annual cycles and the differences in the presence of slow varying cycles with the long characteristic scales  
242 are likely to be influenced by their proximity to the data time span of 6 years (4 years for CI). This implies that the  
243 model evaluation shouldn't go beyond 3 years (2 years for CI) given the current data coverage. CMAQ captured the  
244 3-year cycles in EC and total PM<sub>2.5</sub> and 2-year cycles in OC and CI, despite an overestimation in the scales of 2-year  
245 cycles in observed SO<sub>4</sub> and NO<sub>3</sub>.



246

247 **Fig. 3. The characteristic scales resolved in the IMFs of observed and simulated total and speciated PM<sub>2.5</sub> for**  
248 **(a) QURE, (b) RENO and (c) ATL. IMF1 to the last pair of IMFs with increasing characteristic periods are**  
249 **shown from bottom left to top right. Top left panel in each subplot shows characteristic scales in the unit of**  
250 **years (y-axis) of all IMFs with inter-annual cycles (the x-axis represents the IMF number). In the subplots,**  
251 **species decomposed from observations are connected by solid lines, while species decomposed from simulations**  
252 **are represented by smaller markers in darker shades connected by dashed lines.**

253 Similar features in observed and simulated total and speciated PM<sub>2.5</sub> concentrations at RENO are presented in Fig. 3b.  
254 Likewise, the highest peaks in the power spectrum also sit in the annual cycles of IMF6 except for the observed OC  
255 and total PM<sub>2.5</sub> which have higher peak power at half-year cycles. All annual IMFs are statistically significant except  
256 for simulated NH<sub>4</sub> (Fig. S5). The small variation in the estimated characteristic period of IMF6 is because this  
257 monitoring site is located in a wildfire prone region on the border of Nevada and California. Clear evidence can be  
258 seen from Fig. 4a that an extra annual cycle in the IMF6 of observations in the summer of 2008 is depicted, which is  
259 very possibly driven by the 2008 California Wildfires spanning from May until November. Unlike the diversified  
260 scales in IMF7 at QURE, IMF7 at RENO features universal 2-year cycles of all species as well as total PM<sub>2.5</sub> and all  
261 of them are well replicated by the model. However, variations in time scales are present in IMF8 possibly because of  
262 the limited data coverage. Thus, only species with time scales less than 4 years in both observations and model  
263 simulations are evaluated. It is evident that CMAQ has reproduced the 3-year cycles in SO<sub>4</sub> and NH<sub>4</sub>.



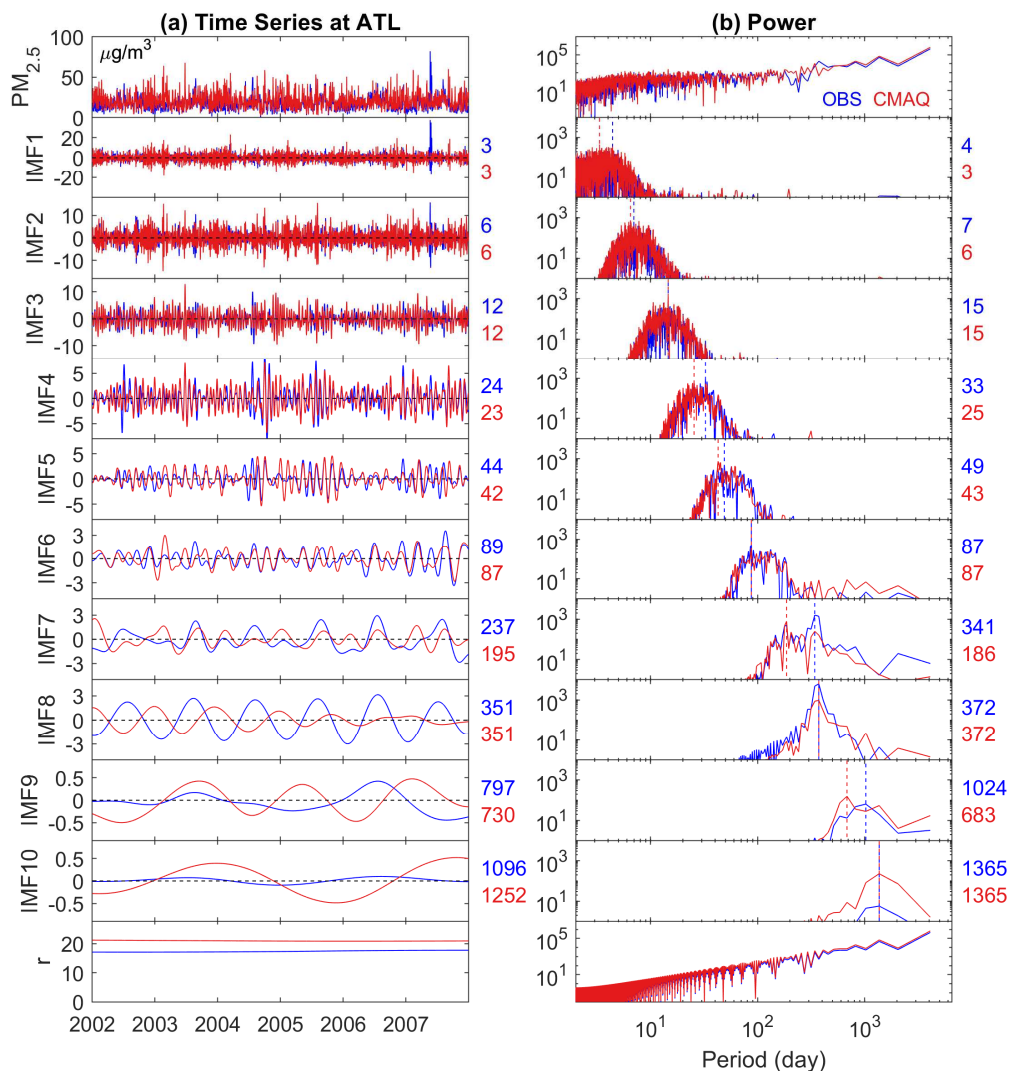
264  
 265 **Fig. 4. Same as Fig. 2 but for the RENO site with 8 IMFs.**

266

267 ATL is the only speciated site with daily data coverage. Observed and simulated total and speciated PM<sub>2.5</sub>  
 268 concentrations at the ATL site are decomposed into 9 or 10 IMFs (Fig. 3c). Because of the change in data frequency,  
 269 high frequency scales such as weekly cycles can be evaluated and the significance tested (Fig. S5) annual cycles with  
 270 the highest peak power is represented by IMF8 (IMF7 for SO<sub>4</sub> and NO<sub>3</sub>). Annual cycles of SO<sub>4</sub> and NO<sub>3</sub> appeared in  
 271 the earlier stage of decomposition in IMF7 because of their relatively weak half-year cycles, which largely led to the  
 272 mixed signal of half year and annual cycles in IMF7 in total PM<sub>2.5</sub> as in Fig. 5b. This is more visible in the observed  
 273 IMF7 where the energy of the one-year period surpasses that of the half year. Yet, clues can be seen from Fig. 5 that  
 274 the amplitude and the energy of annual cycles leaked into IMF7 is very limited compared to that remaining in IMF8,  
 275 indicating that it is still safe to conduct model evaluation on the seasonality using IMF8 with an underestimation in



276 the amplitude of observation. On the other hand, inferences should be made with caution for IMF7 because of the  
277 mixed modes. Scales up to 3 years are relatively well reproduced by the model.



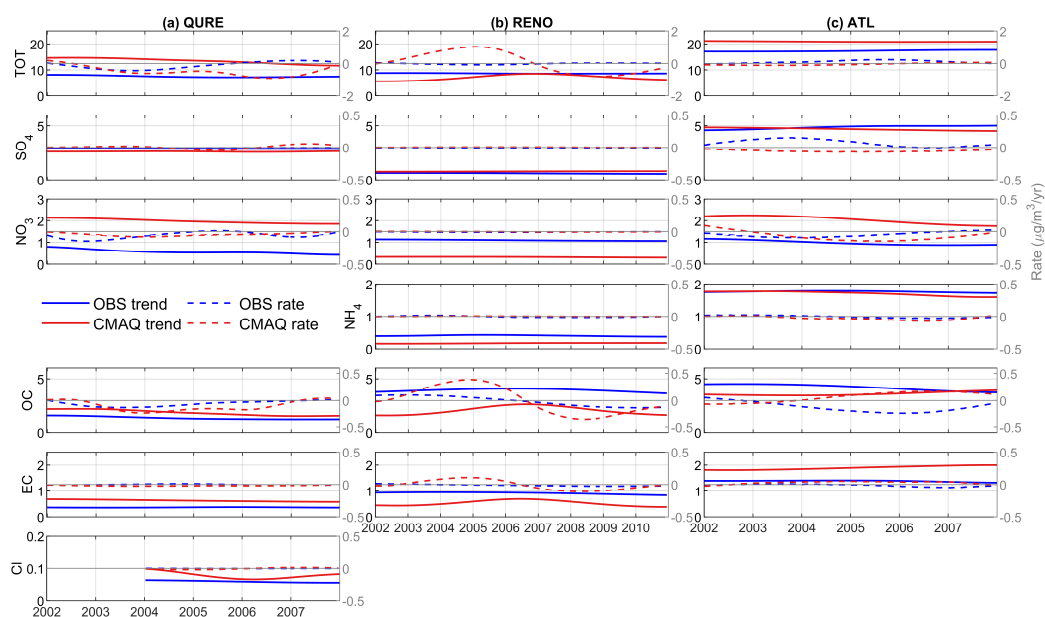
278  
279 **Fig. 5.** Same as Fig. 2 but for the ATL site with 10 IMFs.

## 280 4.2 Long-term trend

281 The EMD-decomposed long-term trend components for the observed and simulated total and speciated PM<sub>2.5</sub>  
282 concentrations are presented in Fig. 6. To better visualize the non-linearity of the trend component,  
283 (temporal derivative of a trend component, which is the change in the consecutive concentration divided by the



284 sampling rate of 1 or 3 days and converted to the unit of  $\mu\text{g}/\text{m}^3/\text{year}$  by multiplying 365 day/year) are added with a  
285 separate y-axis on the right side in each panel (gray colored scale). It is evident that  $\text{PM}_{2.5}$  is changing at a varying  
286 rate, forming either a monotonic trend component or a trend component with one extremum, which cannot be fully  
287 represented by a single constant number using a traditional linear regression approach. Given that there are chemical  
288 species other than the ones studied in the total  $\text{PM}_{2.5}$ , not all performance issues can be fully explained by the five  
289 available species.



290  
291 **Fig. 6.** Trend components of observed and simulated total and speciated  $\text{PM}_{2.5}$  for (a) QURE, (b) RENO and (c)  
292 ATL in  $\mu\text{g}/\text{m}^3$  with dashed lines representing the rate of the change (temporal derivative of the trend component  
293 converted to  $\mu\text{g}/\text{m}^3/\text{year}$ ) against the right-side y axis, with a reference line of no change in dark gray line in  
294 the center.

295 At the QURE site, CMAQ captures the general decreasing trend in observed total  $\text{PM}_{2.5}$  which can mainly be traced  
296 back to  $\text{NO}_3$  and OC, while both observed and simulated trend components in  $\text{SO}_4$  and EC are relatively constant (Fig.  
297 6a). Moreover, the periods with highest decreasing rate in observed total  $\text{PM}_{2.5}$  during 2003-2004 with a decreasing  
298 rate of  $-0.44 \mu\text{g}/\text{m}^3/\text{year}$  is also well replicated by the model. Nevertheless, the slightly increasing  $\text{PM}_{2.5}$  level in the  
299 later years is simulated to be decreasing at a much higher rate, which is partly due to the overestimated decreasing rate  
300 in OC and species other than the five studied ones. The trend component of simulated CI shows a cyclic-like feature  
301 because of proximity between the existence of a cycle of 4-5 years (by decomposing the simulation during the 6-year  
302 study period) and 4-year period limited by the available quality assured observations. The rate of change in the  
303 simulated trend component by decomposing the simulation during the 6-year study period would mimic that from the



304 4-year observation, both with a negligible negative value throughout 2004-2007. However, the magnitude of the trend  
305 component is almost doubled (1.8 times compared with observation) in the model with contribution from all species  
306 except for SO<sub>4</sub>. A quantitative summary of the magnitude of the trend component can be found in Table 1.

307 **Table 1.** The ratio of mean magnitude of the trend component  $r_{trend}$  (CMAQ/observation). Boldface values indicate  
308 a relatively good estimate of the magnitude (0.7 - 1.3). “-” indicates the data is not available (same applies for Tables  
309 2 and 3).

	TOT	SO <sub>4</sub>	NO <sub>3</sub>	NH <sub>4</sub>	OC	EC	Cl
QURE	1.8	<b>0.9</b>	3.5	-	1.4	1.7	<b>1.3</b>
RENO	<b>0.8</b>	<b>1.3</b>	0.3	0.4	0.5	0.6	-
ATL	<b>1.2</b>	<b>1.0</b>	2.1	<b>1.0</b>	<b>0.9</b>	1.4	-

310

311 RENO is located close to the border with California and is affected by large wildfire breakouts in the western U.S. as  
312 can be seen in the spikes of the observed total PM<sub>2.5</sub> (Fig. 4a). The model simulates large increasing rate up to 1.03  
313 μg/m<sup>3</sup>/year and decreasing rate up to -0.80 μg/m<sup>3</sup>/year before and after the 2006-2007 winter season and fails to  
314 reproduce the relative stable condition seen in the observations with only -0.09 μg/m<sup>3</sup>/year decreasing in 2004-2005  
315 and 0.04 μg/m<sup>3</sup>/year increasing in 2008-2009 (Fig. 6b). Similar feature is found for combustion related OC and EC  
316 species. The observed slightly decreasing trends in SO<sub>4</sub> and NH<sub>4</sub> during 2005-2009 are not being captured in the model  
317 simulations. The magnitude of the trend component is slightly underestimated with  $r_{trend}$  of 0.8 with contribution  
318 from all species except for SO<sub>4</sub> as well (Table 1).

319 During the period of 2002-2007, observations at ATL reveal a slightly increasing PM<sub>2.5</sub> trend that cannot be explained  
320 by the five listed PM<sub>2.5</sub> components trend (Fig. 6c), possibly indicating a contribution of the remaining species such  
321 as the non-carbonaceous portion of organic matter. Non-carbonaceous organic matter can account for more than half  
322 of total organic matter, which, in turn, can account for a large portion of the total PM<sub>2.5</sub> mass (Edgerton et al., 2005).  
323 In contrast, the model shows a slight decreasing trend with a peak decreasing rate in 2003 and misses the peak  
324 increasing rate of 0.23 μg/m<sup>3</sup>/year in the winter season of 2005. Similarly, reversed trends are also simulated for SO<sub>4</sub>,  
325 OC and EC, while the change rate in NO<sub>3</sub> is well captured. Unlike the previous sites, magnitude of trend components  
326 in total and speciated PM<sub>2.5</sub> are well simulated except for EC (1.4 times the observation) and NO<sub>3</sub> (2.1 times).

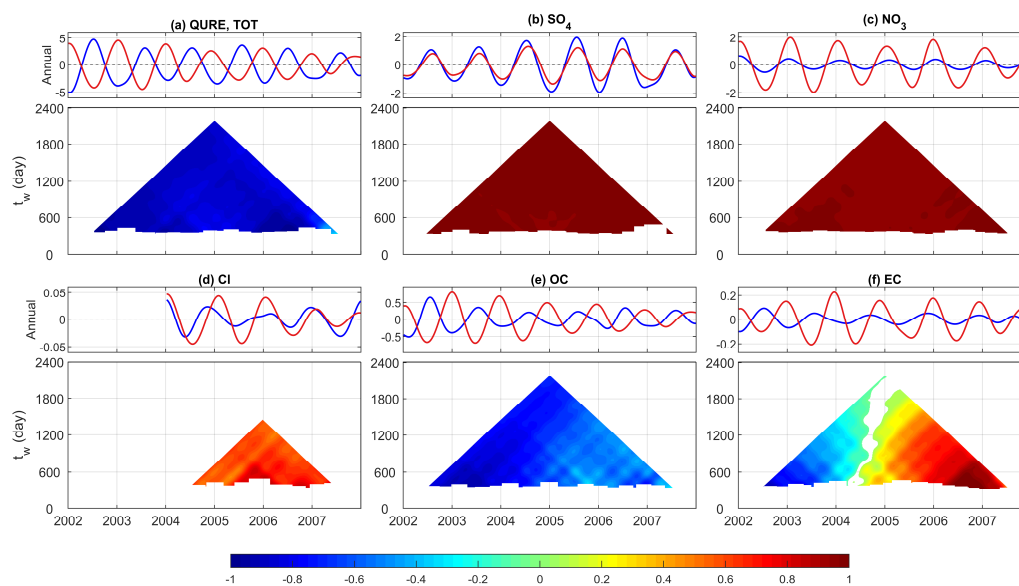
327 To sum up, the long-term trend at QURE is well simulated by the model. The occurrence of large wildfires lasting for  
328 several months have significantly impacted the long-term trend component at RENO and the model failed to capture  
329 those combustion-related species and total PM<sub>2.5</sub> primarily due to limitations in the historical data used to specify day-  
330 specific wildfire emissions (Xing et al., 2013). Slightly increasing levels of PM<sub>2.5</sub> and its species observed at ATL are  
331 simulated to be slightly decreasing, except for NO<sub>3</sub> which is well simulated. The magnitude of the long-term trend  
332 components of total PM<sub>2.5</sub> and SO<sub>4</sub> are well represented by CMAQ (Table 1). The model performs differently across  
333 the sites in terms of the magnitudes of the trend component in NO<sub>3</sub>, NH<sub>4</sub>, Cl, OC and EC. Species other than those in



334 the available dataset may also play a considerable role in driving the agreements or disagreements between model  
335 simulations and observations of total  $\text{PM}_{2.5}$ .

### 336 4.3 Seasonality

337 The EMD-assisted seasonality evaluations utilize the decomposed IMF with characteristic period of one year to  
338 evaluate the amplitude and phase of the model simulation, both of which are time- dependent. We first demonstrate  
339 the evaluation for total  $\text{PM}_{2.5}$  at QURE (Fig. 7a). The top panel shows the annual cycle components and the bottom  
340 panel shows its TDIC pyramid. The decreasing amplitude of the annual cycles throughout 2002-2007 is almost  
341 perfectly represented with an overall ratio  $r_{\text{annual}}$  being 1.0 (Table 2). Each pixel in the TDIC pyramid is the  
342 correlation (color-coded) calculated during a period of time  $I(t)$  with width of  $t_w$  days (y-axis) centered at a specific  
343 day (x-axis) as introduced in Section 3.2. The annual cycle mean periods are identical between CMAQ and  
344 observations (350 days, Fig. 2a IMF6), but there is a phase shift for all years with the entire TDIC pyramid being close  
345 to -1. By shifting the CMAQ annual cycles backward 159 days (almost half year), the overall correlation of the annual  
346 component can reach up to a peak of 0.9 (Table 3).



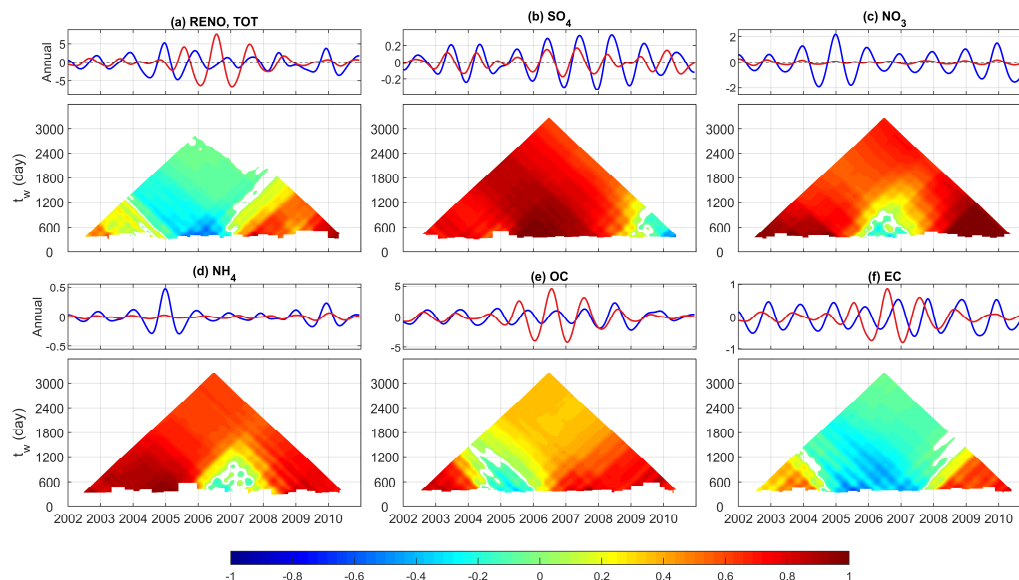
347

348 **Fig. 7. Decomposed annual cycles (IMF6) from observed (blue) and simulated (red) concentrations ( $\mu\text{g}/\text{m}^3$ ) of**  
349 **(a) total  $\text{PM}_{2.5}$ , (b)  $\text{SO}_4$ , (c)  $\text{NO}_3$ , (d) Cl, (e) OC and (f) EC and their corresponding TDIC at Quabbin Summit,**  
350 **MA. The window size  $t_w$  indicates the width of the window used to calculate a specific correlation centered at**  
351 **the day represented in x-axis.**

352 What are the driving factors for the above phase shift in modeled total  $\text{PM}_{2.5}$  at Quabbin Summit, MA? The illustrations  
353 in Fig. 7a for total  $\text{PM}_{2.5}$  alone cannot provide useful information that will allow the modeler to improve the model's  
354 performance. This is accomplished by applying the EMD method to the  $\text{PM}_{2.5}$  speciated components (Fig. 7b-f). Traces



355 of the semi-annual phase shift (-159 days) of annual cycles or large overestimation in the winter and underestimation  
356 in the summer is because of the largely overestimated amplitude of  $\text{NO}_3$  (4.3 times that of observation) which peaks  
357 in the winter and the almost semi-annual shifted OC (-147 days), as well as contributions from EC and Cl.  $\text{NO}_3$  has a  
358 mean amplitude reaching almost half of that of the total  $\text{PM}_{2.5}$ . OC directly drives both the observed and simulated  
359 annual components to be negatively correlated. EC follows the feature of OC in the first four years or so and the  
360 feature of  $\text{NO}_3$  in 2006 and 2007 and contributes to the half year shifted total  $\text{PM}_{2.5}$ . The magnitude of winter-peaking  
361 Cl cycles are overestimated with a phase shift of one month. However, the contribution of Cl is very limited because  
362 of the tiny amplitude in both observed and simulated annual cycles. In addition, annual cycles in  $\text{SO}_4$  are well  
363 reproduced for the entire time span with an amplitude ratio of 0.7. A quantitative summary of the evaluation of the  
364 annual cycles at this site can be found in Tables 2 and 3.



365

366 **Fig. 8.** Same as in Fig. 7 for Reno, NV, except that (d) represents  $\text{NH}_4$  rather than Cl.

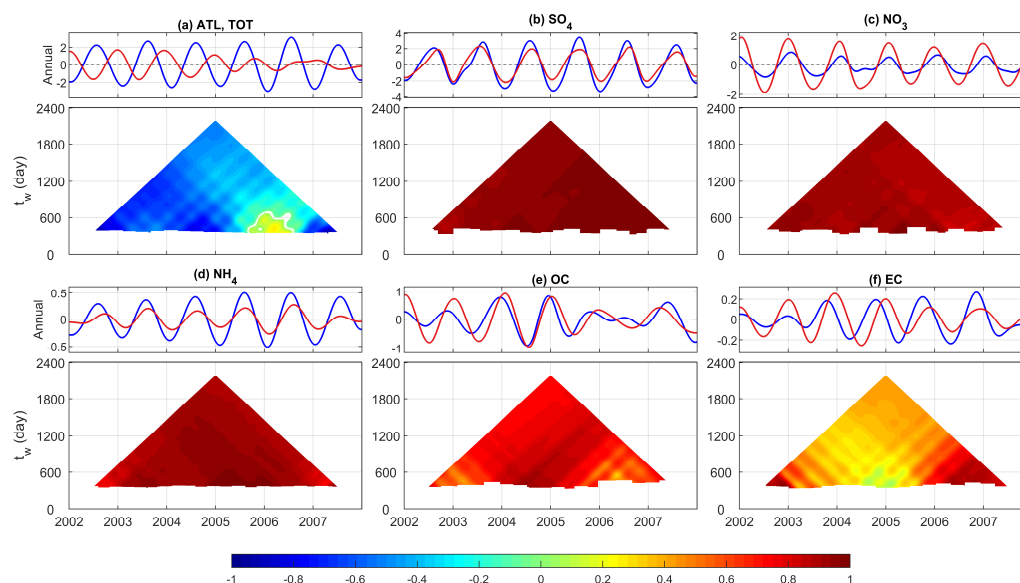
367 Both observed and simulated annual cycles at the RENO site are largely contaminated by the extreme events lasting  
368 for several months that are not properly simulated, indicating the need for more appropriate emissions allocation.  
369 Overall, annual variations for total and speciated  $\text{PM}_{2.5}$  are largely underestimated except for the total  $\text{PM}_{2.5}$  and  
370 combustion-driven EC and OC from 2005 to 2007 (Fig. 8). The modeled phase of  $\text{SO}_4$ ,  $\text{NO}_3$ ,  $\text{NH}_4$  and OC agrees with  
371 that of observation with exception for a length of about two years in each that missed the phasing: 2009-2010 for  $\text{SO}_4$ ,  
372 summer 2005-summer 2007 for  $\text{NO}_3$ , 2006-2007 for  $\text{NH}_4$  and 2004-2005 for OC. It is also notable that the TDIC  
373 pyramid of EC mimics that of total  $\text{PM}_{2.5}$ , implying the existence of errors in modeled EC in processes such as  
374 emissions, transport, and deposition that affected the model performance for total  $\text{PM}_{2.5}$ . In comparison,  $\text{SO}_4$  and OC  
375 are relatively well simulated with a mean amplitude ratio of 0.5 and 1.5 and a phase shift of 36 and 33 days,  
376 respectively.





377 Observed annual cycles of total PM<sub>2.5</sub> at the ATL site features a slightly increasing amplitude of annual variations  
378 from 2002 to 2006 which then decreased to the original state in 2007 (Fig. 9a). Conversely, model-simulated annual  
379 cycles became weaker throughout the period, with an overall  $r_{annual}$  of 0.5. As at the QURE site, the simulated annual  
380 components at the ATL site also show a shift of several months (-132 days). Specifically, traces of these phase shifts  
381 or large overestimation in the winter and underestimation in the summer can be seen from the more than doubled  
382 amplitude of NO<sub>3</sub> which peaks in winter and underestimated SO<sub>4</sub> and NH<sub>4</sub> in the warm seasons as well as the -54 days  
383 shifted EC. The anti-correlated remaining species other than those in the available dataset clearly played a role in  
384 driving the discrepancies seen in the total PM<sub>2.5</sub> annual cycles (Fig. 10). Specifically, the anti-correlation likely points  
385 to an inaccurate representation of the seasonal variation of the non-carbonaceous portion of organic matter due to an  
386 improper representation of organic aerosols in the model version analyzed here; this problem has since been corrected  
387 in more recent releases of the CMAQ model. The underestimated annual variations in the remaining components  
388 closely resemble that of the annual variation in total PM<sub>2.5</sub>. The phase of simulated SO<sub>4</sub>, NO<sub>3</sub>, NH<sub>4</sub>, and OC species is  
389 in good agreement with those in observations and the amplitude of simulated annual cycles in SO<sub>4</sub>, OC and EC agree  
390 well with that in the observations (Tables 2 and 3).

391 In sum, annual cycles of PM<sub>2.5</sub> are also time-dependent and the phase in the annual cycles for total PM<sub>2.5</sub>, OC and EC  
392 reveal a general shift of up to half a year (Table 3); this indicates a potential problem in the allocation of emissions  
393 during this study period and/or the treatment of organic aerosols in this version of the model. CMAQ generally  
394 simulated the phase in SO<sub>4</sub>, NO<sub>3</sub>, Cl and NH<sub>4</sub> quite well but did not always capture the magnitude of their variations  
395 (Table 2).

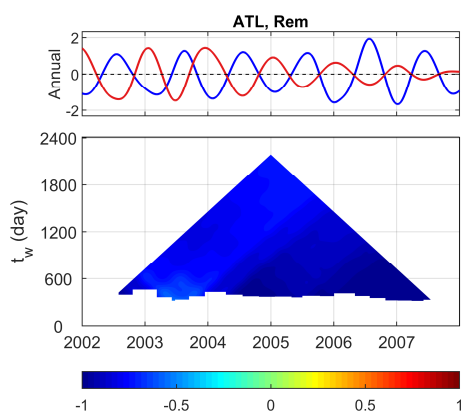


396



397 **Fig. 9.** Same as in Fig. 7 for Atlanta, GA, except that the annual component is resolved in IMF8 (IMF7 for SO<sub>4</sub>  
 398 and NO<sub>3</sub>) because of the difference in sampling rate and characteristic embedded in the time series at ATL and  
 399 (d) represents NH<sub>4</sub> rather than Cl.

400



401

402 **Fig. 10.** Decomposed annual cycles in Atlanta, GA for the remaining components presented in total PM<sub>2.5</sub> other  
 403 than the five species in Fig. 9.

404 **Table 2.** The ratio of mean amplitude of the annual component  $r_{annual}$  (CMAQ/observation). Boldface values indicate  
 405 a magnitude with a ratio close to 1 (0.7 -1.3).

	TOT	SO <sub>4</sub>	NO <sub>3</sub>	NH <sub>4</sub>	OC	EC	Cl
QURE	<b>1.0</b>	<b>0.7</b>	4.3	-	1.6	3.1	1.6
RENO	<b>1.2</b>	0.5	0.1	0.2	1.5	<b>0.9</b>	-
ATL	0.5	<b>0.7</b>	2.4	0.4	<b>1.2</b>	<b>1.0</b>	-

406

407 **Table 3.** Phase shift ( $n$ ) of CMAQ simulated annual cycle components in days. The background color indicates the  
 408 maximum correlation ( $R_{max}$ ) that can be reached by shifting the CMAQ time series  $n$  days with respect to  
 409 observations: white = [0.8, 1], light grey = [0.6, 0.8], grey = [0.4, 0.6], dark grey = (0.2, 0.4). The bold shows number  
 410 of shifts less than a month while the italic shows shifts longer than three months.

	TOT	SO <sub>4</sub>	NO <sub>3</sub>	NH <sub>4</sub>	OC	EC	Cl
QURE	<i>-159</i>	<b>-6</b>	<b>3</b>	-	<i>-147</i>	<i>-105</i>	<b>-30</b>
RENO	<b>78</b>	36	<b>12</b>	<b>-21</b>	33	96	-
ATL	<i>-132</i>	<b>0</b>	<b>8</b>	<b>-17</b>	<b>-24</b>	-54	-

411



#### 412 4.4 Sub-seasonal and inter-annual variability

413 In this section, model performance at multiple sub-seasonal and inter-annual scales with cycles less than 3 years,  
414 presented in the total and speciated  $PM_{2.5}$ , is evaluated following an approach similar to that for the annual cycles in  
415 Section 4.3 (Fig. 11). First, IMFs from observations and model simulations are paired based on their characteristic  
416 periods following the discussion in Section 4.1. Then, the magnitude of specific scales is evaluated using  $r_{IMFn}$   
417 following Equation 6 of the  $r_{annual}$  for annual cycles. The phase shifts of the time series are assessed by the proportion  
418 of shifted days relative to the mean characteristic scales of the corresponding observed and simulated IMFs ( $n/t_m$ ).  
419 For example, a phase shift of 0.1 cycles in the 2-year cycles is approximately 73 days while it would be 18 days for  
420 the half-year cycles.

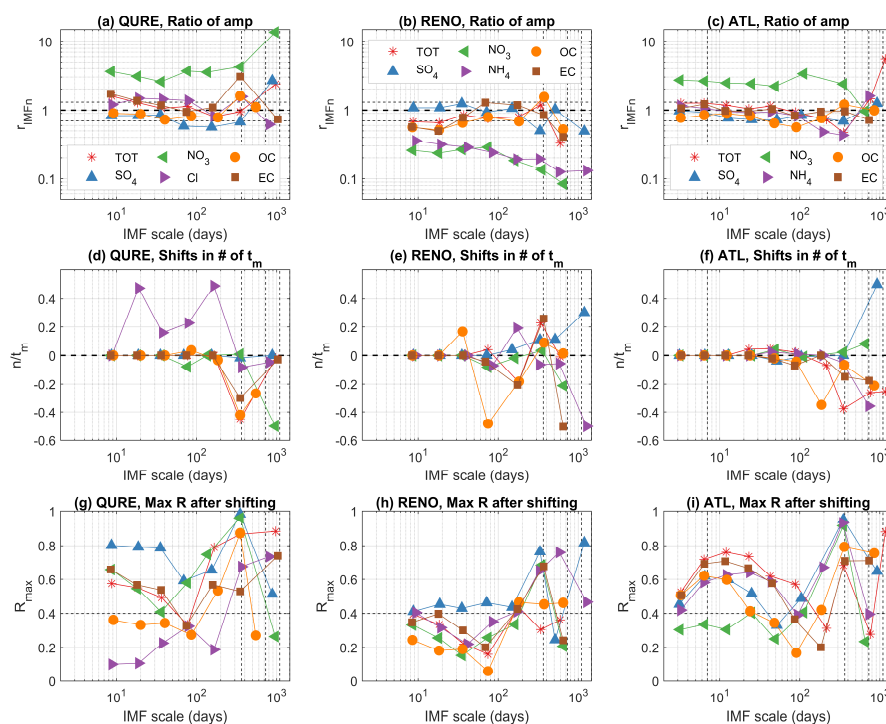
421 The performance of the simulated amplitude of the sub-seasonal and inter-annual cycles is relatively stable from a few  
422 days to semi-annual scales and  $r_{IMFn}$  is close to 1 in most cases (Fig. 11a-c). CMAQ captures the features seen in the  
423 observations at QURE, except for the large overestimation of  $NO_3$  ( $r_{IMFn}$  ranges from 2.6 to 3.7 at the sub-seasonal  
424 scale and reaches up to 13.8 for the 3-year cycles). Similar overestimation of  $NO_3$  is also found at ATL ( $r_{IMFn}$  ranges  
425 from 2.0 to 3.4, except for the 2-year cycles). In contrast,  $NO_3$  at RENO is strongly underestimated with  $r_{IMFn}$  ranging  
426 from 0.1 to 0.3 and reaching its minimum at the 2-year cycles. Likewise, all time scales of  $NH_4$  at RENO are also  
427 being underestimated with  $r_{IMFn}$  decreasing from 0.4 to only 0.1 at the 3-year cycles. The coexistence of  
428 underestimation of  $NO_3$  and  $NH_4$  variability, as well as their trend component, likely points to the insufficient grid  
429 resolution in representing ammonium nitrate episodes associated with stagnant meteorology in the mountainous  
430 regions as illustrated by Kelly et al. (2019). To sum up, model has simulated the magnitude of features across all scales  
431 in most of the studied cases. However, fluctuations in  $NO_3$  are constantly being largely over- or under-estimated and  
432 improvements to the model are required to better replicate its variability (Fig. 11a-c).

433 A high  $R_{max}$  of corresponding IMFs can only be achieved when the characteristic scales of those from observations  
434 and model simulations are close, there is minimal mode mixing, and negligible irregular change of amplitude exists  
435 during the study period. Thus,  $R_{max}$  tends to be small for all oscillations at RENO because of the irregular impact  
436 from events such as wildfires. Thus, the interpretation of phase shift is focused on the components and time scales  
437 having correlations above 0.4 only.

438 Results show that the sub-seasonal cycles at QURE all have a negligible phase shift of less than 0.1 cycles (Fig. 11d).  
439 The semi-annual cycles at RENO have around 0.2 cycle phase shifts in total  $PM_{2.5}$  (-0.2),  $NH_4$ (0.2), OC (-0.2), and  
440 EC (-0.2) while negligible phase shifts of less than 0.1 cycles are simulated in  $SO_4$  ranging from 9 days to semi-annual  
441 in scale. As at QURE, multiple sub-seasonal cycles at ATL all have a negligible phase shift of less than 0.1 cycles,  
442 with the exception of semi-annual OC which has a phase shift of nearly -0.4 cycles with a marginal correlation of  
443 around 0.4. Unlike the relatively stable  $R_{max}$  throughout the time scales within each of the species for QURE and  
444 RENO, the  $R_{max}$  at ATL tends to be much higher (roughly 0.6-0.8) in the scales of 6 to 25 days, except for  $NO_3$ ,  
445 indicating the model's success in simulating those weather-induced air quality fluctuations at this site as reflected by  
446 their negligible phase shifts.



447 However, the physical meaning of each sub-seasonal IMF is not yet fully understood and requires further study.  
 448 Synoptic scale IMFs (IMFs with scale less than/around a month) usually have large variance and are not statistically  
 449 significant different from white noise except for observed  $\text{SO}_4$  and  $\text{NH}_4$  (Fig. S5). Yet, observed and simulated total  
 450 and some speciated  $\text{PM}_{2.5}$  at QURE and ATL (except IMF1) can achieve moderate to high  $R_{max}$  at these time scales  
 451 (Fig. 11 g-i), indicating a potential physical explanation of those time scales using meteorological variables. IMFs  
 452 with scales longer than a month but less than half year possess much less variance and are usually not statistically  
 453 significant different from noise. Exceptions are also found at the Atlanta site where observed IMFs are mostly  
 454 significant different from noise. Whereas semi-annual cycles are mostly statistically significant (note that semi-annual  
 455  $\text{SO}_4$  and  $\text{NO}_3$  at ATL are too weak to be decomposed into a separate IMF). In a previous study, He et al. (2014) found  
 456 semi-annual oscillations in the corrected AERosol RObotic NETwork (AERONET) Aerosol Optical Depth (AOD) and  
 457  $\text{PM}_{10}$  mass concentrations are primarily caused by the change of wind directions in Hong Kong.



458

459 **Fig. 11. Model performance at all temporal scales for sites QURE, RENO and ATL. (a-c) ratio of mean**  
 460 **amplitude of corresponding IMFs with similar characteristic mean periods (ideal ratio=1.0); (d-f) the phase**  
 461 **shift  $n$  in the number of mean periods (average mean period of corresponding IMFs decomposed from**  
 462 **observation and model simulation); (g-i) maximum correlation  $R_{max}$  can be achieved by shifting the modeled**  
 463 **time series. The average mean period of corresponding IMFs decomposed from observations and CMAQ of**  
 464 **total and speciated  $\text{PM}_{2.5}$  are represented on the x-axis; all metrics on the y-axis are unitless. Horizontal**



465 **reference lines are drawn at 0.7 and 1.3 in (a-c). Weekly, annual and inter-annual (2- to 3-year) scales are**  
466 **marked with vertical dashed lines.**

467 The evaluation and interpretation of inter-annual cycles are constrained by the limited available speciated observations  
468 for a period of 6 to 9 years (4 years for Cl at QURE). Thus, only 2- to 3-year cycles are presented (Fig. 11) and  
469 evaluated. Among the 2- to 3-year inter-annual cycles at QURE, there is minimal phase shift for total PM<sub>2.5</sub>, SO<sub>4</sub>, Cl,  
470 and EC with moderate to high  $R_{max}$ . At RENO, the model presents negligible shifts in 2-year cycles of OC and NH<sub>4</sub>  
471 while phase shifts of 0.3 and -0.5 cycles are simulated in the 3-year cycles for SO<sub>4</sub> and NH<sub>4</sub>. At ATL, the phase shift  
472 of -0.2 to -0.4 cycles are simulated for PM<sub>2.5</sub>, NH<sub>4</sub>, OC, and EC with periods of 2- to 3-year cycles; while 2- to 3-year  
473 SO<sub>4</sub> cycles have a half-year cycle shift.

## 474 **5 Conclusions**

475 The main advantage for using EMD to evaluate PM<sub>2.5</sub> and its speciated components is that it decomposes nonlinear  
476 and nonstationary signals into multiple modes and a residual trend component. It does not require any preselection of  
477 the temporal scales and assumptions of linearity and stationarity for the data, thereby providing insights into time  
478 series of PM<sub>2.5</sub> concentrations and its components. Using improved CEEMDAN, we are able to assess how well  
479 regional-scale air quality models like CMAQ can simulate the intrinsic time-dependent long-term trend and cyclic  
480 variations in daily average PM<sub>2.5</sub> and its species. This type of coordinated decomposition and evaluation of total and  
481 speciated PM<sub>2.5</sub> provides a unique opportunity for modelers to assess influences of each PM<sub>2.5</sub> species to the total  
482 PM<sub>2.5</sub> concentration in terms of time shifts for various temporal cycles and the magnitude of each component including  
483 the trend.

484 A demonstration of how improved CEEMDAN could be applied to time series data at three sites over CONUS that  
485 provide speciated PM<sub>2.5</sub> data reveals the presence of the annual cycles in PM<sub>2.5</sub> concentrations and time-dependent  
486 features in all decomposed components. At these three sites, the model generally is more capable of simulating the  
487 change rate in the trend component than the absolute magnitude of the long-term trend component. However, the  
488 magnitude of SO<sub>4</sub> trend components is well represented across all three sites. Also, the model reproduced the amplitude  
489 of the annual cycles for total PM<sub>2.5</sub>, SO<sub>4</sub> and OC. The phase difference in the annual cycles for total PM<sub>2.5</sub>, OC and  
490 EC reveal a shift of up to half-year, indicating the need for proper allocation of emissions and an updated treatment  
491 of organic aerosols compared to the earlier model version used in this set of model simulations. The consistent large  
492 under/over-prediction of NO<sub>3</sub> variability at all temporal scales and magnitude in the trend component, as well as the  
493 abnormally low correlations of synoptic scale NO<sub>3</sub> at ATL, calls for better representation of nitrate partitioning and  
494 chemistry. Wildfires have the potential to elevate PM<sub>2.5</sub> for months and can alter its variability at scales from few days  
495 to the entire year. Thus, more accurate fire emission data should be incorporated to improve model simulation,  
496 especially in those fire-prone regions.

497 **Data availability.** Paired observations and CMAQ model data used in the analysis will be made available at  
498 <https://edg.epa.gov/metadata/catalog/main/home.page>. Raw CMAQ model outputs are available on request from the  
499 U.S EPA authors.



500 **Author contribution.** "HL and MA designed the methodology; RM, CH and SR contributed in the assessment of the  
501 outcomes and were consulted on necessary revisions. Model simulations were performed by the US EPA. HL prepared  
502 the manuscript with contributions from all co-authors."

### 503 **Acknowledgements**

504 The views expressed in this paper are those of the authors and do not necessarily represent the view or policies of the  
505 U.S. Environmental Protection Agency. Two of the authors (MA and HL) acknowledge that part of this work was  
506 supported by the Electric Power Research Institute (EPRI) Contract #00-10005071, 2015–2017.

### 507 **References**

508 Astitha, M., Luo, H., Rao, S.T., Hogrefe, C., Mathur, R., Kumar, N., 2017. Dynamic evaluation of two decades of  
509 WRF-CMAQ ozone simulations over the contiguous United States. *Atmospheric Environment* 164, 102–116.

510 Banzhaf, S., Schaap, M., Kraneburg, R., Manders, A.M.M., Segers, A.J., Visschedijk, A.H.J., Denier van der on,  
511 H.A.C., Kuenen, J.P.P., van Meijgaard, E., van Ulft, L.H., Cofala, J., Builtjes, P.J.H., 2015. Dynamic model evaluation  
512 for secondary inorganic aerosol and its precursors over Europe between 1990 and 2009. *Geoscientific Model*  
513 *Development* 8, 1047–1070.

514 Chang, P.C., Flatau, A., Liu, S.C., 2003. Review Paper: Health Monitoring of Civil Infrastructure. *Structural Health*  
515 *Monitoring* 2, 257–267.

516 Chen, X., Wu, Z., Huang, N.E., 2010. The time-dependent intrinsic correlation based on the empirical mode  
517 decomposition. *Adv. Adapt. Data Anal.* 02, 233–265.

518 Civerolo, K., Hogrefe, C., Zalewsky, E., Hao, W., Sistla, G., Lynn, B., Rosenzweig, C., Kinney, P.L., 2010. Evaluation  
519 of an 18-year CMAQ simulation: Seasonal variations and long-term temporal changes in sulfate and nitrate.  
520 *Atmospheric Environment* 44, 3745–3752.

521 Colominas, M.A., Schlotthauer, G., Torres, M.E., 2014. Improved complete ensemble EMD: A suitable tool for  
522 biomedical signal processing. *Biomedical Signal Processing and Control* 14, 19–29.

523 Derot, J., Schmitt, F.G., Gentilhomme, V., Morin, P., 2016. Correlation between long-term marine temperature time  
524 series from the eastern and western English Channel: Scaling analysis using empirical mode decomposition. *Comptes*  
525 *Rendus Geoscience* 348, 343–349.

526 Edgerton, E.S., Hartsell, B.E., Saylor, R.D., Jansen, J.J., Hansen, D.A., Hidy, G.M., 2005. The Southeastern Aerosol  
527 Research and Characterization Study: Part II. Filter-Based Measurements of Fine and Coarse Particulate Matter Mass  
528 and Composition. *Journal of the Air & Waste Management Association* 55, 1527–1542.

529 Foley, K.M., Hogrefe, C., Pouliot, G., Possiel, N., Roselle, S.J., Simon, H., Timin, B., 2015. Dynamic evaluation of  
530 CMAQ part I: Separating the effects of changing emissions and changing meteorology on ozone levels between 2002  
531 and 2005 in the eastern US. *Atmospheric Environment* 103, 247–255.



- 532 Gan, C.-M., Pleim, J., Mathur, R., Hogrefe, C., Long, C.N., Xing, J., Wong, D., Gilliam, R., Wei, C., 2015. Assessment  
533 of long-term WRF–CMAQ simulations for understanding direct aerosol effects on radiation “brightening” in the  
534 United States. *Atmospheric Chemistry and Physics* 15, 12193–12209.
- 535 Hansen, D.A., Edgerton, E.S., Hartsell, B.E., Jansen, J.J., Kandasamy, N., Hidy, G.M., Blanchard, C.L., 2003. The  
536 Southeastern Aerosol Research and Characterization Study: Part 1—Overview. *Journal of the Air & Waste*  
537 *Management Association* 53, 1460–1471.
- 538 He, J., Zhang, M., Chen, X., & Wang, M., 2014. Inter-comparison of seasonal variability and nonlinear trend between  
539 AERONET aerosol optical depth and PM10 mass concentrations in Hong Kong. *Science China Earth*  
540 *Sciences*, 57(11), 2606–2615.
- 541 Henneman, L.R.F., Liu, C., Hu, Y., Mulholland, J.A., Russell, A.G., 2017. Air quality modeling for accountability  
542 research: Operational, dynamic, and diagnostic evaluation. *Atmospheric Environment* 166, 551–565.
- 543 Hogrefe, C., Hao, W., Zalewsky, E.E., Ku, J.-Y., Lynn, B., Rosenzweig, C., Schultz, M.G., Rast, S., Newchurch, M.J.,  
544 Wang, L., Kinney, P.L., Sistla, G., 2011. An analysis of long-term regional-scale ozone simulations over the  
545 Northeastern United States: variability and trends. *Atmospheric Chemistry and Physics* 11, 567–582.
- 546 Huang, N.E., Shen Zheng, Long Steven R., Wu Manli C., Shih Hsing H., Zheng Quanan, Yen Nai-Chyuan, Tung Chi  
547 Chao, Liu Henry H., 1998. The empirical mode decomposition and the Hilbert spectrum for nonlinear and non-  
548 stationary time series analysis. *Proceedings of the Royal Society of London. Series A: Mathematical, Physical and*  
549 *Engineering Sciences* 454, 903–995.
- 550 Huang, Y., Schmitt, F.G., 2014. Time dependent intrinsic correlation analysis of temperature and dissolved oxygen  
551 time series using empirical mode decomposition. *Journal of Marine Systems* 130, 90–100.
- 552 Kang, D., Hogrefe, C., Foley, K.L., Napelenok, S.L., Mathur, R., Trivikrama Rao, S., 2013. Application of the  
553 Kolmogorov–Zurbenko filter and the decoupled direct 3D method for the dynamic evaluation of a regional air quality  
554 model. *Atmospheric Environment* 80, 58–69.
- 555 Kelly, J.T., Koplitz, S.N., Baker, K.R., Holder, A.L., Pye, H.O.T., Murphy, B.N., Bash, J.O., Henderson, B.H., Possiel,  
556 N.C., Simon, H., Eyth, A.M., Jang, C., Phillips, S., Timin, B., 2019. Assessing PM2.5 model performance for the  
557 conterminous U.S. with comparison to model performance statistics from 2007–2015. *Atmospheric Environment* 214,  
558 116872.
- 559 Mathur, R., Xing, J., Gilliam, R., Sarwar, G., Hogrefe, C., Pleim, J., Pouliot, G., Roselle, S., Spero, T.L., Wong, D.C.,  
560 Young, J., 2017. Extending the Community Multiscale Air Quality (CMAQ) Modeling System to Hemispheric Scales:  
561 Overview of Process Considerations and Initial Applications. *Atmos Chem Phys* 17, 12449–12474.
- 562 Moghtaderi, A., Borgnat, P., Flandrin, P., 2012. Gap-filling by the empirical mode decomposition, in: 2012 IEEE  
563 International Conference on Acoustics, Speech and Signal Processing (ICASSP). Presented at the 2012 IEEE  
564 International Conference on Acoustics, Speech and Signal Processing (ICASSP), pp. 3821–3824.





- 565 Rato, R.T., Ortigueira, M.D., Batista, A.G., 2008. On the HHT, its problems, and some solutions. *Mechanical Systems*  
566 *and Signal Processing*, Special Issue: *Mechatronics* 22, 1374–1394.
- 567 Torres, M.E., Colominas, M.A., Schlotthauer, G., Flandrin, P., 2011. A complete ensemble empirical mode  
568 decomposition with adaptive noise, in: 2011 IEEE International Conference on Acoustics, Speech and Signal  
569 Processing (ICASSP). Presented at the 2011 IEEE International Conference on Acoustics, Speech and Signal  
570 Processing (ICASSP), pp. 4144–4147.
- 571 White, W.H., 2008. Chemical markers for sea salt in IMPROVE aerosol data. *Atmospheric Environment* 42, 261–  
572 274.
- 573 Wong, D.C., Pleim, J., Mathur, R., Binkowski, F., Otte, T., Gilliam, R., Pouliot, G., Xiu, A., Young, J.O., Kang, D.,  
574 2012. WRF-CMAQ two-way coupled system with aerosol feedback: software development and preliminary results.  
575 *Geoscientific Model Development* 5, 299–312.
- 576 Wu, Z., Huang, N.E., 2004. A study of the characteristics of white noise using the empirical mode decomposition  
577 method. *Proceedings of the Royal Society of London. Series A: Mathematical, Physical and Engineering Sciences*  
578 460, 1597–1611.
- 579 Wu, Z., Huang, N.E., 2009. Ensemble empirical mode decomposition: a noise-assisted data analysis method. *Adv.*  
580 *Adapt. Data Anal.* 01, 1–41.
- 581 Wu, Z., Huang, N.E., Long, S.R., Peng, C.-K., 2007. On the trend, detrending, and variability of nonlinear and  
582 nonstationary time series. *PNAS* 104, 14889–14894.
- 583 Xing, J., Mathur, R., Pleim, J., Hogrefe, C., Gan, C.-M., Wong, D.C., Wei, C., Gilliam, R., Pouliot, G., 2015.  
584 Observations and modeling of air quality trends over 1990–2010 across the Northern Hemisphere: China, the United  
585 States and Europe. *Atmospheric Chemistry and Physics* 15, 2723–2747.
- 586 Xing, J., Pleim, J., Mathur, R., Pouliot, G., Hogrefe, C., Gan, C.-M., Wei, C., 2013. Historical gaseous and primary  
587 aerosol emissions in the United States from 1990 to 2010. *Atmospheric Chemistry and Physics* 13, 7531–7549.
- 588 Yahya, K., Wang, K., Campbell, P., Glotfelty, T., He, J., Zhang, Y., 2016. Decadal evaluation of regional climate, air  
589 quality, and their interactions over the continental US using WRF/Chem version 3.6.1. *Geoscientific Model*  
590 *Development* 9, 671–695.
- 591 Yeh, J.-R., Shieh, J.-S., Huang, N.E., 2010. Complementary ensemble empirical mode decomposition: a novel noise  
592 enhanced data analysis method. *Adv. Adapt. Data Anal.* 02, 135–156.
- 593 Yu, L., Wang, S., Lai, K.K., 2008. Forecasting crude oil price with an EMD-based neural network ensemble learning  
594 paradigm. *Energy Economics* 30, 2623–2635.
- 595 Zhou, W., Cohan, D.S., Napelenok, S.L., 2013. Reconciling NO<sub>x</sub> emissions reductions and ozone trends in the U.S.,  
596 2002–2006. *Atmospheric Environment* 70, 236–244.